



Modeling and optimization of a typical fuel cell–heat engine hybrid system and its parametric design criteria

Yingru Zhao, Jincan Chen*

Department of Physics and Institute of Theoretical Physics and Astrophysics, Xiamen University, Xiamen 361005, People's Republic of China

ARTICLE INFO

Article history:

Received 10 August 2008

Accepted 19 September 2008

Available online 1 October 2008

Keywords:

Fuel cell

Heat engine

Hybrid system

Irreversibility

Performance analysis

Optimum criteria

ABSTRACT

A theoretical modeling approach is presented, which describes the behavior of a typical fuel cell–heat engine hybrid system in steady-state operating condition based on an existing solid oxide fuel cell model, to provide useful fundamental design characteristics as well as potential critical problems. The different sources of irreversible losses, such as the electrochemical reaction, electric resistances, finite-rate heat transfer between the fuel cell and the heat engine, and heat-leak from the fuel cell to the environment are specified and investigated. Energy and entropy analyses are used to indicate the multi-irreversible losses and to assess the work potentials of the hybrid system. Expressions for the power output and efficiency of the hybrid system are derived and the performance characteristics of the system are presented and discussed in detail. The effects of the design parameters and operating conditions on the system performance are studied numerically. It is found that there exist certain optimum criteria for some important parameters. The results obtained here may provide a theoretical basis for both the optimal design and operation of real fuel cell–heat engine hybrid systems. This new approach can be easily extended to other fuel cell hybrid systems to develop irreversible models suitable for the investigation and optimization of similar energy conversion settings and electrochemistry systems.

© 2008 Elsevier B.V. All rights reserved.

1. Introduction

Nowadays the development of clean energy systems, for both transportation and stationary applications, is recognized as mandatory to satisfy well-known environmental and regulatory requirements in terms of emissions and energy conversion efficiencies. Because of their high efficiencies and zero toxic emission levels, fuel cell systems are considered as one of the most attractive solutions in the automotive and power generation industry. Among the existing fuel cell technologies, the high-temperature fuel cells show a great promise due to their high energy conversion efficiency, fuel flexibility and high temperature of the exhaust heat which allows favorable co-generation and combination with other types of power generators such as heat engines [1–4].

After the concept of fuel cell–heat engine hybrid systems was proposed at early 1990, a number of investigations have been carried out about the system performance from the energetic point of view [5–7]. In a group of works [8–10], the cell performance was evaluated based on the operating curve interpolated from experimental test results. Some authors [5,6,11] performed

a parametric analysis to understand the effects of different operating conditions on the performance of a specified system. Most of the papers are dealing with the theoretical cycle analysis and simulation of the possible configurations of the hybrid systems [11,12].

Since it is difficult to experimentally quantify the interrelated parameters governing a hybrid system, theoretical modeling and numerical analysis become essential for the optimization of the system design and operating conditions. Therefore, the purpose of the present paper is to clarify these issues and present a general and fundamental analysis of the theoretical performance potential of a fuel cell–heat engine hybrid system.

Based on the simplifying assumptions derived from literature and performance data provided in [13], an irreversible thermodynamic modeling for a fuel cell–heat engine hybrid system is further carried out to simulate the system response to the changes in the operating conditions and design parameters through parametric study. The different sources of energy losses are specified and the performance characteristics of the system are investigated. In particular, both the heat-leak from the fuel cell to the environment and heat transfer between the fuel cell and the heat engine are considered. As a consequence, the performance of the hybrid system is optimized. These findings indicate which parts of the system deserve the greatest effort if one wants to improve the overall cycle efficiency.

* Corresponding author. Tel.: +86 592 2180922; fax: +86 592 2189426.
E-mail address: jcchen@xmu.edu.cn (J. Chen).

2. An irreversible model of the fuel cell–heat engine hybrid systems

Although fuel cell technology has been studied extensively, the best way to employ fuel cell unites for the generation of electrical power remains to be determined. Optimal thermal management allows for effective use of the system’s byproduct, heat, leading to substantial increases in the overall system efficiency. The heat generated in a fuel cell may be dissipated by convection, conduction or radiation. However, mostly the heat may be used to run a thermodynamic cycle, such as a heat engine, for additional power generation.

It is our opinion that initially a fuel cell–heat engine hybrid system has to be as simple as possible to achieve competitive first cost, and, probably even more important, high reliability and availability. Thus, an illustration of a simplified fuel cell–heat engine hybrid system is shown in Fig. 1, where fuel cell acts as the high-temperature heat reservoir of a heat engine for a further production of power. The role of the regenerator in the hybrid system is to preheat the incoming fuel and air with the high-temperature exhaust gas of the fuel cell and to ensure that the fuel cell works at steady-state. This model is helpful to understand the architecture of any combined cycle of fuel cells and heat engines and can be easily expanded to analyze different chemical reaction processes.

The whole hybrid system is formulated based on the following general simplifications and assumptions [13–18]:

1. Both the fuel cell and heat engine are assumed to operate under steady-state conditions.
2. All gases are assumed to be ideal.
3. Perfect regeneration is considered for the heat exchanger.
4. Operating temperature and pressure are uniform and constant for the fuel cell domain including the inlet reactants and outlet products.
5. Complete chemical reactions are considered and no reactants are remained after the reaction.

With the help of these assumptions, the governing equations of this hybrid model will be presented in this section as the influence of some new parameters is considered.

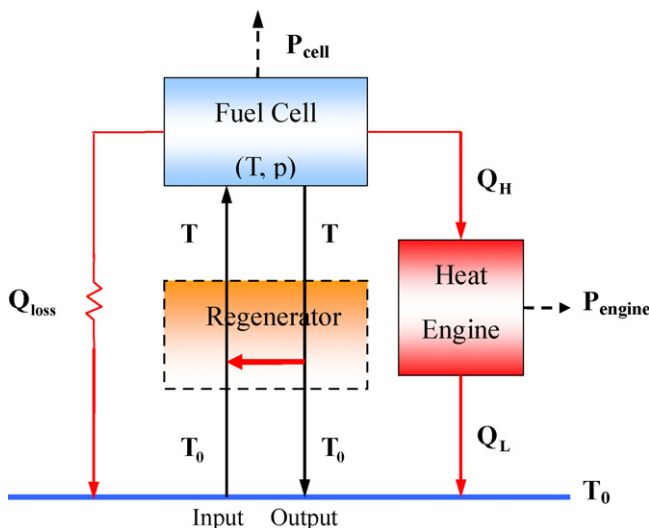


Fig. 1. The schematic diagram of a typical fuel cell–heat engine hybrid system.

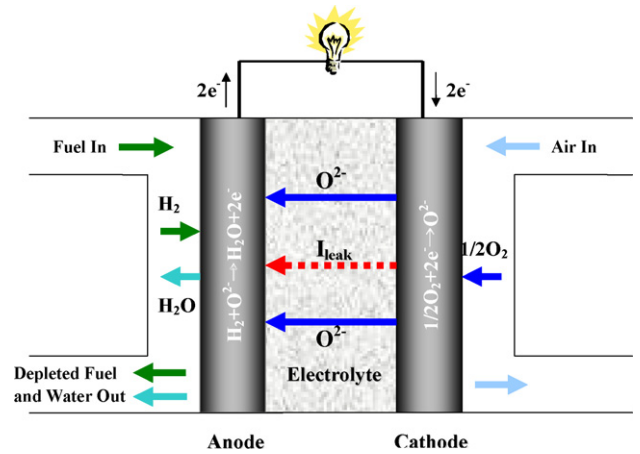


Fig. 2. The schematic diagram of a hydrogen–oxygen solid oxide fuel cell.

2.1. A fuel cell model

The fuel cell model presented in this study has been reported in Ref. [13], which is based on a solid oxide fuel cell (SOFC) using hydrogen as fuel and air as oxidant. The basic working principle is illustrated in Fig. 2. The overall electrochemical reaction in such a cell can be summarized as $H_2 + (1/2)O_2 \rightarrow H_2O + \text{Heat} + \text{Electricity}$.

It is well-known that the measured open-circuit potential in a practical fuel cell is usually lower than the ideal reversible potential, because there always exist some irreversible losses originating primarily from activation overpotential (V_{act}), ohmic overpotential (V_{ohm}), and concentration overpotential (V_{conc}) [16,19–24]. One way to handle this behavior is to assume some electronic current leakage through the electrolyte [21,25–29]. Thus, a leakage resistance can be introduced, which is in parallel with the external load. When electrons flow through the internal and external fuel cell circuit, the local behavior of the irreversible losses is described as a simple equivalent electrical circuit, which is series of a reversible voltage determined by the Nernst equation, an internal resistance made up by the sum of three overpotential contributions, and a leakage resistance in parallel with the load.

The maximum electrical work obtainable in a fuel cell, operating at constant temperature (T) and pressure ($p_0 = 1 \text{ atm}$), is given by the change in Gibb’s free energy ($-\Delta G$) of the electrochemical reaction. The relationship between the Gibb’s free energy (G) and the reaction enthalpy (H) is known to be

$$-\Delta H = -\Delta G - T \Delta S \quad (1)$$

where $\bar{Q} = -\Delta H$ corresponds to the total thermal energy available in the system, ΔS denotes the change in entropy and $-T\Delta S$ represents the amount of heat generated by a fuel cell operating reversibly. The enthalpy change and Gibbs free energy change between the products and the reactants of the global electrochemical reaction at temperature T for the steady-state fuel cell can be, respectively, expressed as

$$\Delta \dot{H} = \frac{iA}{n_e F} \Delta h \quad (2)$$

and

$$\Delta \dot{G} = \frac{iA}{n_e F} \Delta g(T, p) \quad (3)$$

where $\Delta h = \sum_k v_k h_k - \sum_j v_j h_j$, $\Delta g(T, p) = \sum_k v_k \mu_k(T, p) - \sum_j v_j \mu_j(T, p)$, n_e is the number of electrons transferred in reaction, i is the current density, A is the surface area of the polar plate (supposing that the bipolar plates have the same area), $F = 96,485 \text{ C mol}^{-1}$ is Faraday's constant, h is the molar enthalpy of the species, μ is the partial molar Gibbs free energy of species (which is also the chemical potential), v is the stoichiometric coefficient for species, and subscripts k and j represent the k th product and j th reactant of the reaction, respectively. Specifically, $\Delta g(T, p) = \Delta g^\circ(T) - RT \ln(p_{\text{H}_2} p_{\text{O}_2}^{1/2} / p_{\text{H}_2\text{O}})$ denotes the molar Gibbs free energy change for the fuel cell reaction, where $R = 8.314 \text{ J mol}^{-1} \text{ K}^{-1}$ is the universal gas constant, p_{H_2} , p_{O_2} , and $p_{\text{H}_2\text{O}}$ are the partial pressures of reactants H_2 , O_2 , and H_2O , respectively. It is noteworthy that $\Delta g^\circ(T) = \Delta h^\circ - T \Delta s^\circ$ is the molar Gibbs free energy change at $p_0 = 1 \text{ atm}$ and is, therefore, called the standard molar Gibbs free energy change, which also depends on temperature [14,16,19,23,30,31], and that the calculation of $\Delta g^\circ(T)$ is based on the tabulated values [32] at operating temperature T .

Since the Gibbs free energy change of an electrochemical reaction is a measure of the maximum electrical energy obtainable from the reaction [30], the maximum (reversible) power output generated by the reaction in the fuel cell can be determined by

$$P_{rev} = -\Delta \dot{G} = -\frac{iA}{n_e F} \Delta g(T, p) \quad (4)$$

As mentioned previously, Eq. (4) is a measure of the maximum work obtainable from the reaction in the reversible fuel cell. In practice, this part of energy is never completely utilized because of the various thermodynamic and electrochemical irreversibilities [33,34]. When the fuel cell works normally and produces useful power through the external load, combining those irreversibilities yields the rate of the total entropy production of an irreversible fuel cell, which includes the entropy production rate resulting from the internal resistance and leakage resistance as

$$\dot{S}_{tot} = \frac{I_{int}^2 R_{int}}{T_0} + \frac{I_{leak}^2 R_{leak}}{T_0} \quad (5)$$

where T_0 is the ambient temperature, I_{int} and I_{leak} represent the corresponding electric currents through the equivalent internal resistance R_{int} and the leakage resistance R_{leak} , respectively.

With considering all the irreversibilities discussed in the above analysis, the power output of the fuel cell can be deduced from Eqs. (4) and (5) as [13]

$$P_{cell} = -\Delta \dot{G} - T_0 \dot{S}_{tot} = \frac{iA}{n_e F} \left(m - \frac{k}{RTd_1} m^2 \right) \quad (6)$$

where

$$d_1 = 2n_e \sinh^{-1} \left(\frac{i}{2i_{0,a}} \right) + 2n_e \sinh^{-1} \left(\frac{i}{2i_{0,c}} \right) - \ln \left(1 - \frac{i}{i_{l,a}} \right) - \ln \left(1 - \frac{i}{i_{l,c}} \right) + \frac{i n_e F L_{el}}{\sigma_0 R} \exp \left(\frac{E_{el}}{RT} \right), \quad k = R_{int} / R_{leak},$$

$$\text{and } m = -\Delta h^\circ + T \Delta s^\circ + RT \ln \left(\frac{p_{\text{H}_2} p_{\text{O}_2}^{1/2}}{p_{\text{H}_2\text{O}}} \right) - RTd_1$$

For any energy-conversion device that takes in energy to produce work, the basic definition of thermal efficiency is the useful work output divided by the total energy input [35–37]. Thus, from the thermodynamic point of view, the efficiency of the irreversible

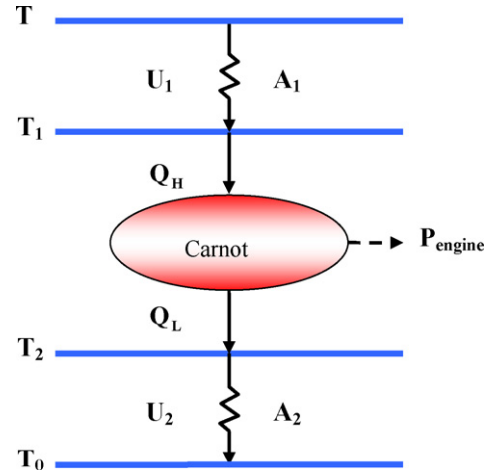


Fig. 3. The schematic diagram of an endoreversible Carnot heat engine.

fuel cell can be defined as

$$\eta_{cell} = \frac{P_{cell}}{\dot{Q}} = \frac{P_{cell}}{-\Delta \dot{H}} = \frac{P_{cell}}{-(iA/n_e F) \Delta h^\circ} = \frac{1}{-\Delta h^\circ} \left(m - \frac{k}{RTd_1} m^2 \right) \quad (7)$$

2.2. An endoreversible Carnot heat engine

For a practical heat engine, there are invariably thermal resistances between the working substance and the external heat reservoirs. For the sake of convenience, the heat engine in the hybrid system is assumed to be an endoreversible Carnot cycle [38], as shown in Fig. 3, where the heat \dot{Q}_H is transferred from the high-temperature heat reservoir (fuel cell) at T to the working fluid at T_1 , and \dot{Q}_L from the working fluid at T_2 to the environment at T_0 . When the heat transfer between the reservoirs and the working fluid is assumed to obey Newton's law [39], we have

$$\dot{Q}_H = U_1 A_1 (T - T_1) \quad (8)$$

and

$$\dot{Q}_L = U_2 A_2 (T_2 - T_0) \quad (9)$$

where U_1 and U_2 denote the overall heat-transfer coefficients between the working fluid and the heat reservoirs, and A_1 and A_2 are the heat-transfer areas between the working fluid and the heat reservoirs.

As illustrated in Fig. 2, a part of the waste heat produced in the fuel cell is directly released as heat-leak (\dot{Q}_{loss}) to the environment [7,39–42], which may be expressed as [43]

$$\dot{Q}_{loss} = KA_l (T - T_0) \quad (10)$$

where K is the convective and/or conductive heat-leak coefficient, and A_l denotes the effective heat-transfer area. Combining the previous analysis and above equations yields

$$\dot{Q}_H = -\Delta \dot{H} - P_{cell} - \dot{Q}_{loss} = -\Delta \dot{H} - P_{cell} - KA_l (T - T_0) \quad (11)$$

According to the definition of an endoreversible Carnot cycle, one has $\dot{Q}_H/T_1 = \dot{Q}_L/T_2$ [39,44]. Using the above equations, it can be proved that when $A_1/A_2 = \sqrt{U_2/U_1}$, the optimum efficiency and power output of the heat engine at given \dot{Q}_H and A_h may be expressed as

$$\eta_{engine} = 1 - T_0 / (T - \dot{Q}_H / m_1) = 1 - \frac{1}{[T/T_0 - i m_2 (1 - \eta_{cell}) + m_3 (T/T_0 - 1)]} \quad (12)$$

and

$$P_{engine} = \dot{Q}_H \eta_{engine} = m_1 [im_2 T_0 (1 - \eta_{cell}) - m_3 (T - T_0)] \times \left\{ 1 - \frac{1}{[T/T_0 - im_2(1 - \eta_{cell}) + m_3(T/T_0 - 1)]} \right\} \quad (13)$$

where

$$m_1 = A_h U_1 U_2 / (\sqrt{U_1} + \sqrt{U_2})^2, \quad m_2 = -\frac{A \Delta h^\circ}{n_e F m_1 T_0}, \quad m_3 = \frac{KA_l}{m_1}$$

and $A_h = A_1 + A_2$ denote the overall heat-transfer area of the heat engine [38].

2.3. An ideal regenerative heat exchanger

As illustrated in Fig. 1, the regenerator in the hybrid system works as a heat exchanger, heating the inlet reactants from the ambient temperature to the cell temperature by using the high-temperature outlet gas of the fuel cell. For the sake of simplicity, the regeneration process is assumed to be ideal. This assumption is reasonable, because the efficiency of regenerators with the values of 98–99% have already been reported [45–47]. With the help of perfect regeneration, the fuel cell and hence the whole hybrid system can be ensured to work normally and continually under the condition of steady-state.

2.4. The efficiency and power output of the hybrid system

Combining Eqs. (7) and (11)–(13) yields the following expressions of the efficiency and power output for the hybrid system as

$$\eta_{hybrid} = \frac{P_{hybrid}}{\dot{Q}_{in}} = \frac{P_{cell} + P_{engine}}{-\Delta \dot{H}} = \eta_{cell} + \frac{P_{engine}}{-\Delta \dot{H}} = \eta_{cell} + \frac{\dot{Q}_H P_{engine}}{-\Delta \dot{H} \dot{Q}_H} = \eta_{cell} + [1 - \eta_{cell} - (T/T_0 - 1)m_3/(m_2i)] \times \left\{ 1 - \frac{1}{[T/T_0 - im_2(1 - \eta_{cell}) + m_3(T/T_0 - 1)]} \right\} \quad (14)$$

and

$$P_{hybrid} = \dot{Q}_{in} \eta_{hybrid} = P_{cell} + P_{engine} = \left(-\frac{iA}{n_e F} \Delta h^\circ \right) \left\langle \eta_{cell} + \left[1 - \eta_{cell} - \left(\frac{T}{T_0} - 1 \right) \frac{m_3}{(m_2i)} \right] \times \left\{ 1 - \frac{1}{[T/T_0 - im_2(1 - \eta_{cell}) + m_3(T/T_0 - 1)]} \right\} \right\rangle \quad (15)$$

From Eqs. (14) and (15), it is clearly seen that the efficiency and power output of the hybrid system are closely dependent on the irreversible losses including the irreversibilities within the fuel cell itself and originating from the heat transfer due to convection/conduction in the fuel cell–heat engine hybrid system. In the next section, numerical predictions will be studied to outline how the irreversible model based on the above analysis can provide a valuable tool for improving the system performance.

3. General performance characteristics and optimal criteria

Optimal design and analysis of a system require a thorough understanding of its performance limitations. It can be seen from Eqs. (14) and (15) that the performance of the fuel cell–heat engine hybrid system depends on a set of thermodynamic and electrochemical parameters such as the operating temperature (T) and the

Table 1
Operating conditions and performance-related parameters [20,48–52].

Parameter	Value
Operating pressure, p_0 (atm)	1
Fuel composition, $p_{H_2}; p_{H_2O}$	0.97; 0.03
Air composition, $p_{O_2}; p_{N_2}$	0.21; 0.79
Charge-transfer coefficient, β	0.5
Number of electrons, n_e	2
Pre-factor for anode exchange current density, γ_a ($A m^{-2}$)	5.5×10^8
Activation energy of anode, $E_{act,a}$ ($J mol^{-1}$)	1.0×10^5
Pre-factor for cathode exchange current density, γ_c ($A m^{-2}$)	7.0×10^8
Activation energy of cathode, $E_{act,c}$ ($J mol^{-1}$)	1.2×10^5
Electrolyte thickness, L_{el} (μm)	20
Activation energy of O^{2-} , E_{el} ($J mol^{-1}$)	8.0×10^4
Pre-factor of O^{2-} , σ_0 ($S m^{-1}$)	3.6×10^7
Ratio of the internal resistance to the leakage resistance, k	1/100
Anode limiting current density, $i_{L,a}$ ($A m^{-2}$)	2.99×10^4
Cathode limiting current density, $i_{L,c}$ ($A m^{-2}$)	2.16×10^4
Faraday constant, F ($C mol^{-1}$)	96,485
Universal gas constant, R ($J mol^{-1} K^{-1}$)	8.314
Standard molar enthalpy change at 1073 K, Δh° ($J mol^{-1}$)	-24,8303
Standard molar entropy change at 1073 K, Δs° ($J mol^{-1} K^{-1}$)	-55.5666

current density (i) of the fuel cell, the parameters related to the heat transfer between the fuel cell and the heat engine and the heat-leak to the surroundings, i.e., m_1 , m_2 , and m_3 . Numerical calculations are performed based on the parameters summarized in Table 1, which are derived from data available in literatures [20,48–52]. Their values are kept constant unless mentioned specifically. The fuel composition is taken as 97% H_2 + 3% H_2O , and the typical oxygen composition in the ambient air, i.e., 21% O_2 + 79% N_2 , is used as oxidant. Moreover, the enthalpy and entropy of reaction are generally not strong functions of temperature, which has been justified by the numerical examples [35,37] for hydrogen–oxygen reaction. Thus, we can invoke the assumption that the changes in enthalpy and entropy across the reaction are independent of temperature.

By using Eqs. (14) and (15), the power density and efficiency of the fuel cell–heat engine hybrid system operating at a temperature range of 1000–1500 K and a current density range of 0–21600 $A m^{-2}$ are presented in Figs. 4 and 5, where the parameters $m_2 = 0.0001 m^2 A^{-1}$ and $m_3 = 0.001$ are chosen, and the power density $P_{hybrid}^* = P_{hybrid}/A$. It can be clearly seen from Figs. 4 and 5 that for the hybrid system, there exist a maximum power output P_{max} and a maximum efficiency η_{max} as the current density i and operating temperature T are varied. Eqs. (14) and (15) show clearly that when Δh° is assumed to be independent of temperature, there is a common extremal condition of $\partial \eta_{hybrid} / \partial T = \partial P_{hybrid} / \partial T = 0$ for the hybrid system. It implies the fact that there is a common optimum temperature T_{opt} for the power output and efficiency of the system. This characteristic is illustrated more clearly in Figs. 4b and 5b. Thus, in the practical operation of the fuel cell–heat engine hybrid system, engineers should search an optimal temperature of the fuel cell carefully to make sure that the whole system works at the optimum condition.

Eqs. (14) and (15) also show that there exist two extremal conditions of $\partial \eta_{hybrid} / \partial i = 0$ and $\partial P_{hybrid} / \partial i = 0$ for the hybrid system, but $\partial \eta_{hybrid} / \partial i \neq \partial P_{hybrid} / \partial i$. It means that the current density at the maximum efficiency (i_η) cannot be equal to that at the maximum power output (i_p), as shown in Fig. 6, where η_m and P_m are

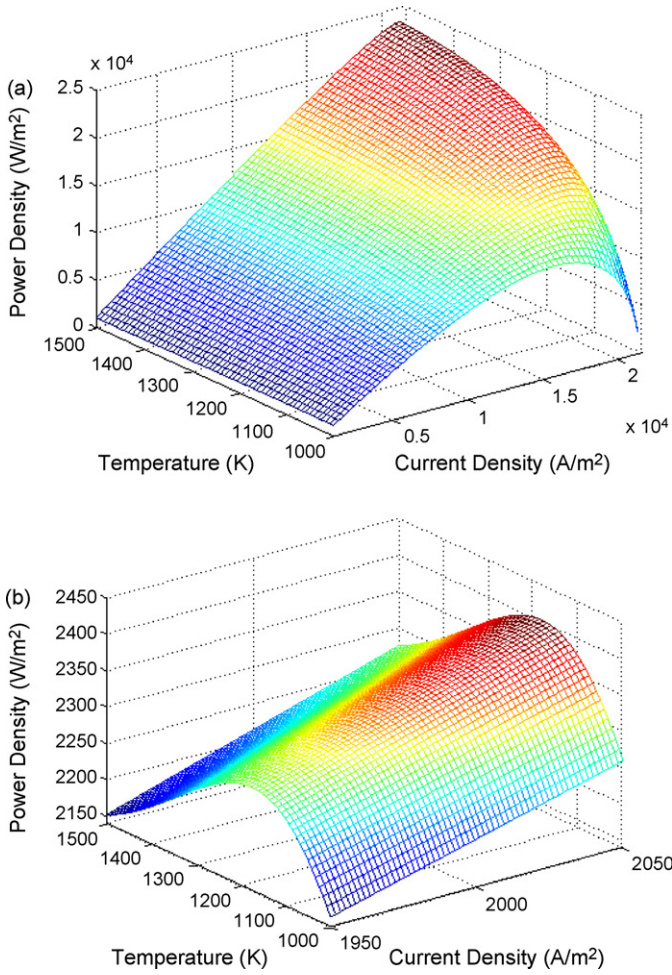


Fig. 4. The power output density as a function of the current density and temperature of the fuel cell, where the parameters $m_2 = 0.0001 \text{ m}^2 \text{ A}^{-1}$ and $m_3 = 0.001$ are chosen. The values of other parameters are listed in Table 1.

the efficiency at the maximum power output and the power output at the maximum efficiency, respectively. It is seen from Fig. 6 that in the region of $i < i_\eta$, the efficiency and power output of the system will decrease as the current density i is decreased; while in the region of $i > i_p$, the efficiency and power output of the system will also decrease as the current density i is increased. It is thus obvious that the regions of $i < i_\eta$ and $i > i_p$ are not optimal from the thermodynamic point of view although the hybrid system may be operated in these regions. Therefore, the optimal region of the current density i for the fuel cell–heat engine hybrid system should be

$$i_\eta \leq i \leq i_p \tag{16}$$

It shows that i_η and i_p are two important parameters of the hybrid system, which determine, respectively, the upper and lower bounds of the optimized current density. In the practical operation of the fuel cell–heat engine hybrid system, engineers should choose a reasonable current density according to Eq. (16) to ensure that the system is operated at the optimal region.

According to the optimum criterion of the current density and Fig. 6, one can further determine the optimum regions for the efficiency and power output as

$$P_m \leq P_{\text{hybrid}} \leq P_{\text{max}} \tag{17}$$

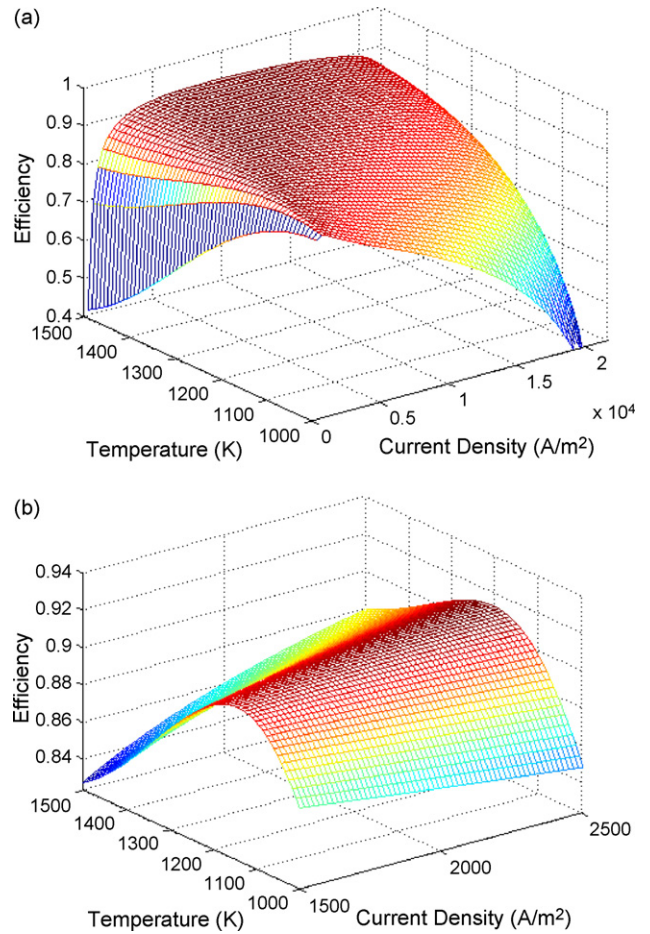


Fig. 5. The efficiency as a function of the current density and temperature of the fuel cell. The values of the relevant parameters are the same as those used in Fig. 4.

and

$$\eta_m \leq \eta_{\text{hybrid}} \leq \eta_{\text{max}} \tag{18}$$

When the hybrid system is operated in these optimum regions, the power output will increase as the efficiency is decreased, and vice versa. The above results show that P_{max} , η_{max} , P_m , and η_m are

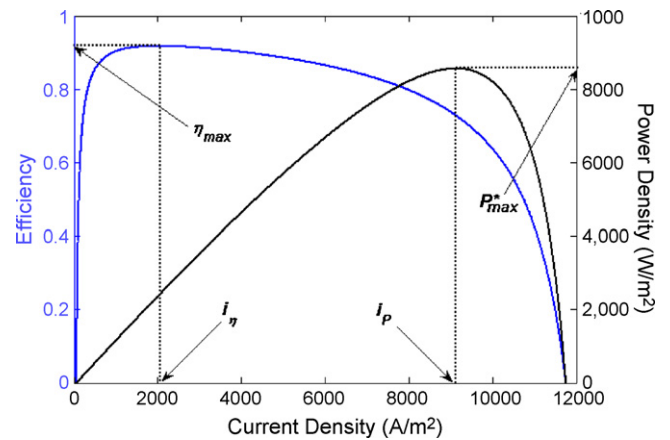


Fig. 6. The curves of efficiency and power density varying with the current density of the fuel cell–heat engine hybrid system for the parameters $T = 1183 \text{ K}$ and $m_2 = 0.00063 \text{ m}^2 \text{ A}^{-1}$, where i_η and i_p are the current densities at the maximum efficiency η_{max} and maximum power output density P_{max}^* , respectively. The values of other parameters are the same as those used in Fig. 4.

also four important parameters of the fuel cell–heat engine hybrid system. P_{\max} and η_{\max} determine the upper bounds of the power output and efficiency of the system, while P_m and η_m determine the allowable optimum values of the lower bounds of the power output and efficiency. Obviously, the four important parameters depend closely on some of the system parameters and can be numerically calculated for the given values of these parameters.

4. Results and discussion

It is noteworthy that the developed system model can be used to investigate the effect of the various operating and design parameters on the performance of the hybrid system. In this section, a parametric analysis is carried out based on the performance criteria for the variation of operating conditions to characterize the system behavior.

4.1. Effect of m_1 and m_3

By using Eqs. (14) and (15), it can be easily proved that the power output and efficiency of the hybrid system are monotonically increasing functions of m_1 . Its physical meaning is quite clear. Because m_1 is a parameter to measure the irreversibility of finite-rate heat transfer in the heat engine, the larger the parameter m_1 , the smaller the heat transfer irreversibility in the heat engine and the better the performance of the hybrid system.

From Eqs. (14) and (15), it can be also proved that the power output and efficiency of the hybrid system are monotonically decreasing functions of m_3 . Its physical meaning may be easily explained as follows: m_3 is a synthesized parameter to measure the heat-leak irreversibility from the fuel cell to the surroundings and the heat transfer irreversibility in the heat engine. The smaller the parameter KA_f is and the larger the parameter m_1 is, i.e., the smaller the heat-leak irreversibility of the fuel cell and the heat transfer irreversibility in the heat engine are, the smaller the parameter m_3 is, and consequently, the better the performance of the hybrid system will be.

4.2. Effect of m_2

The parameter m_2 is a colligation measurement for the systemic structure. By using Eqs. (14) and (15), it may be proved that there is a common extremal condition of $\partial\eta_{\text{hybrid}}/\partial m_2 = \partial P_{\text{hybrid}}/\partial m_2 = 0$ for the hybrid system. It implies the fact that for given values of the current density i and temperature T of the fuel cell, there is a common optimum $(m_2)_{\text{opt}}$ at which both the power output and efficiency attain their maxima, as shown in Fig. 7, where $(m_2)_\eta$ and $(m_2)_P$ are the values of m_2 when the current density is equal to i_η and i_P , respectively. According to Eq. (16), we can further determine the optimal region of the parameter m_2 as

$$(m_2)_P \leq (m_2)_{\text{opt}} \leq (m_2)_\eta \quad (19)$$

Obviously, $(m_2)_\eta$ and $(m_2)_P$ are two important parameters of the hybrid system, which determine, respectively, the upper and lower bounds of the optimized parameter $(m_2)_{\text{opt}}$.

4.3. Effect of m_3/m_2

When $m_1 \rightarrow \infty$, $m_2 = 0$ and $m_3 = 0$, but $m_3/m_2 = (n_e FKA_f T_0)/(-A \Delta h^\circ)$ is a parameter which is independent of m_1 . In fact, m_3/m_2 is only a parameter to measure the performance of the fuel cell and is independent of the heat engine. Figs. 8 and 9 show clearly the effect of m_3/m_2 on the power output and efficiency of the system under the condition of $m_1 \rightarrow \infty$. It

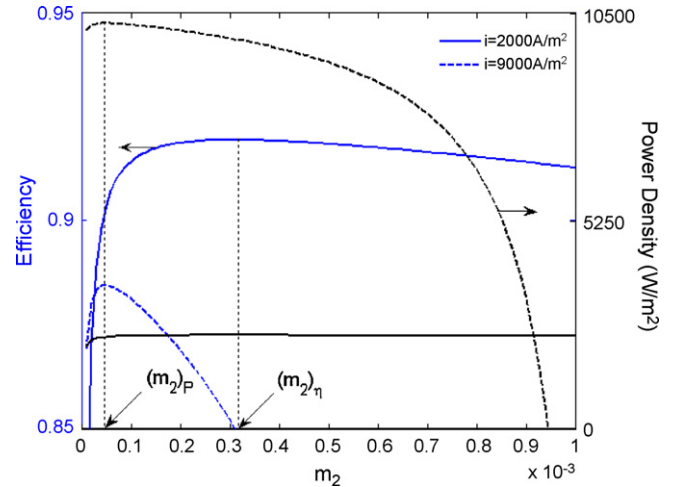


Fig. 7. The curves of the efficiency and power density of the hybrid system varying with m_2 for the parameters $T = 1183 \text{ K}$, $m_3 = 0.001$, where $(m_2)_\eta$ and $(m_2)_P$ are the values of m_2 when the current density is equal to i_η and i_P , respectively. The values of other parameters are the same as those used in Fig. 4.

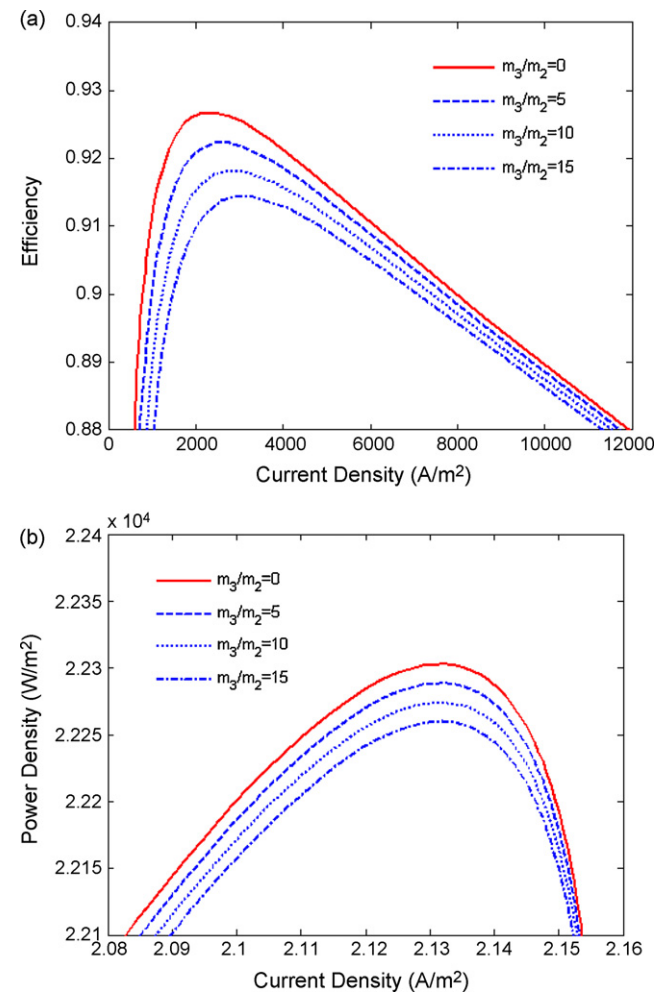


Fig. 8. The curves of (a) the efficiency and (b) power output density of the hybrid system varying with current density of the fuel cell for differently given values of m_3/m_2 , where parameters $m_2 = 0$, $m_3 = 0$, $T = 1183 \text{ K}$, and the values of other parameters are the same as those used in Fig. 4.

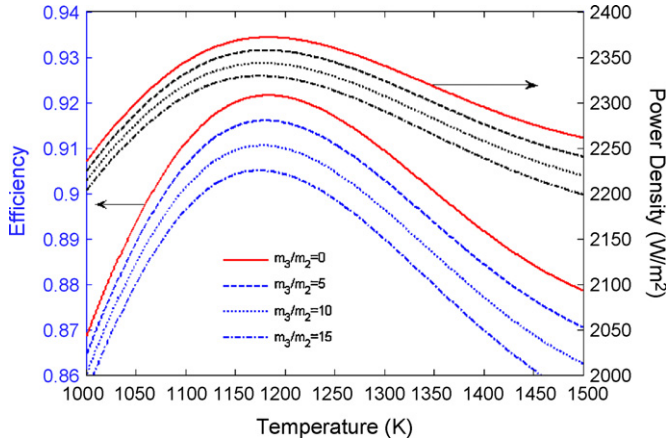


Fig. 9. The curves of the efficiency and power density of the hybrid system varying with the fuel cell temperature for differently given values of m_3/m_2 , where parameters $m_2 = 0$, $m_3 = 0$, $i = 2000 \text{ A m}^{-2}$, and the values of other parameters are the same as those used in Fig. 4.

is observed from Figs. 8 and 9 that both the power output and efficiency of the system will increase obviously as the value of m_3/m_2 is decreased. The reason is quite obvious. The smaller the heat-leak loss from the fuel cell to the surroundings and the larger the enthalpy change, the smaller the parameter m_3/m_2 , and consequently, the better the performance of the hybrid system.

4.4. Several interesting cases

- (1) When the influence of the heat transfer irreversibility in the heat engine is negligible, i.e., the overall heat-transfer coefficients U_1 and U_2 tend to infinity, $m_1 \rightarrow \infty$, $m_2 = 0$, $m_3 = 0$, and Eqs. (12), (14) and (15) may be, respectively, simplified as

$$\eta_{\text{engine}} = 1 - \frac{T_0}{T} = \eta_C \quad (20)$$

$$\eta_{\text{hybrid}} = \eta_{\text{cell}} + \left[1 - \eta_{\text{cell}} - \left(\frac{m_4}{i} \right) \left(\frac{T}{T_0} - 1 \right) \right] \eta_C \quad (21)$$

and

$$P_{\text{hybrid}} = \left(-\frac{iA}{n_e F} \Delta h^\circ \right) \left\{ \eta_{\text{cell}} + \left[1 - \eta_{\text{cell}} - \left(\frac{m_4}{i} \right) \left(\frac{T}{T_0} - 1 \right) \right] \eta_C \right\} \quad (22)$$

where η_C is the Carnot efficiency and $m_4 = m_3/m_2 = (n_e F K A_l T_0) / (-A \Delta h^\circ)$. In such a case, there still exist the maximum values for the power output and efficiency of the hybrid system and the optimal values of the current density and operating temperature of the fuel cell, as shown in Figs. 8 and 9. However, in a practical fuel cell–heat engine hybrid system, the overall heat-transfer coefficients U_1 and U_2 are always finite. m_1 cannot tend to infinity and m_3 is always larger than zero. Thus, the results obtained by using Eqs. (14) and (15) to analyze the performance of a fuel cell–heat engine hybrid system will have more realistic meaning for the optimal design of the system.

- (2) When the heat-leak from the fuel cell to the environment is negligible, i.e., $K A_l \rightarrow 0$, $m_3 = 0$, and Eqs. (12), (14) and (15) may be simplified as

$$\eta_{\text{engine}} = 1 - \frac{1}{[T/T_0 - im_2(1 - \eta_{\text{cell}})]} \quad (23)$$

$$\eta_{\text{hybrid}} = 1 - \frac{1 - \eta_{\text{cell}}}{T/T_0 - im_2(1 - \eta_{\text{cell}})} \quad (24)$$

and

$$P_{\text{hybrid}} = \left(-\frac{iA}{n_e F} \Delta h^\circ \right) \left[1 - \frac{1 - \eta_{\text{cell}}}{T/T_0 - im_2(1 - \eta_{\text{cell}})} \right] \quad (25)$$

- (3) When both the irreversibilities due to the heat transfer between the fuel cell and the heat engine and the heat-leak from the fuel cell to the environment are negligible, i.e., $m_2 = 0$, $m_3 = 0$, and $m_3/m_2 = 0$, we can obtain a simple system model, and consequently, the results obtained above can be simplified. For example, Eqs. (14) and (15) can be, respectively, rewritten as

$$\eta_{\text{hybrid}} = \eta_{\text{cell}} + (1 - \eta_{\text{cell}})\eta_C \quad (26)$$

and

$$P_{\text{hybrid}} = \left(-\frac{iA}{n_e F} \Delta h^\circ \right) [\eta_{\text{cell}} + (1 - \eta_{\text{cell}})\eta_C] \quad (27)$$

As shown clearly by the solid curves in Figs. 8 and 9, the heat-leak does indeed have an obvious effect on the power output and efficiency of the hybrid system.

- (4) When the fuel cell of the hybrid system is totally irreversible, it means that the fuel cell works at the open (or short) circuit condition. In such a case, $P_{\text{cell}} = 0$ and $\eta_{\text{cell}} = 0$, but the heat engine still works normally, and the hybrid system has an efficiency and power output represented by the following equations:

$$\eta_{\text{hybrid}} = \left[1 - \left(\frac{T}{T_0} - 1 \right) \frac{m_3}{(m_2 i)} \right] \times \left\{ 1 - \frac{1}{[T/T_0 - im_2 + m_3(T/T_0 - 1)]} \right\} \quad (28)$$

and

$$P_{\text{hybrid}} = P_{\text{engine}} = \left(-\frac{i_l A}{n_e F} \Delta h^\circ \right) \left[1 - \left(\frac{T}{T_0} - 1 \right) \frac{m_3}{(m_2 i)} \right] \times \left\{ 1 - \frac{1}{[T/T_0 - im_2 + m_3(T/T_0 - 1)]} \right\} \quad (29)$$

- (5) When the heat engine of the hybrid system is totally irreversible, $P_{\text{engine}} = 0$, and consequently, the hybrid system reduces to the simple system of the pure fuel cell and its optimal performance has been given in Ref. [13].

To sum up, by comparing the results obtained by the hybrid system with those derived from the simple systems only with the fuel cell or the heat engine, it is easily seen that the performance of the hybrid system is much better than that of the simple systems. It indicates that the fuel cell–heat engine hybrid power system is an obvious choice for the practical applications.

5. Conclusions

The present paper shows a concept of integrating a heat engine into an existing fuel cell model. It focuses on the system modeling of the fuel cell–heat engine hybrid and tries to improve the whole system performance through numerical simulations. The various irreversible thermodynamic and electrochemical losses are identified, and the individual contribution of these irreversibilities to the whole system performance is investigated through parametric study. The optimum criteria of some important parameters such as the power output and efficiency of the system, the current density and operating temperature of the fuel cell, and the parameters related to the systemic structure are given. Consequently, the performance characteristics of the hybrid system are described and optimized from a thermodynamic point of view. This new method may be easily extended to other fuel cell hybrid systems to develop irreversible models suitable for the optimal energy-management strategies of fuel cell hybrids.

Acknowledgment

This work was supported by the National Natural Science Foundation, People's Republic of China.

References

- [1] S.C. Singhal, K. Kendal, *High Temperature Solid Oxide Fuel Cell: Fundamentals Design and Applications*, Elsevier Ltd., Oxford, 2003.
- [2] M.C. Williams, *Stationary Power Fuel Cell Commercialization Status Worldwide, 1996 Fuel Cell Seminar*, Fuel Cell Seminar Organizing Committee, Washington, DC, 1996, pp. 1–3.
- [3] W. Winkler, H. Lorenz, *J. Power Sources* 106 (2002) 338–343.
- [4] C. Haynes, *J. Power Sources* 92 (2001) 199–203.
- [5] S.H. Chan, H.K. Ho, Y. Tian, *J. Power Sources* 109 (2002) 111–120.
- [6] S.H. Chan, H.K. Ho, Y. Tian, *J. Power Sources* 114 (2003) 213–227.
- [7] S.H. Chan, H.K. Ho, Y. Tian, *Int. J. Hydrogen Energy* 28 (2003) 889–900.
- [8] S. Campanari, *J. Power Sources* 92 (2001) 26–34.
- [9] W. Zang, E. Croiset, P.L. Douglas, M.W. Fowler, E. Entchev, *Energy Convers. Manage.* 46 (2005) 181–196.
- [10] W.J. Yang, S.K. Park, T.S. Kim, J.H. Kim, J.L. Sohn, S.T. Ro, *J. Power Sources* 160 (2006) 462–473.
- [11] J. Palsson, A. Selimovic, L. Sjunnesson, *J. Power Sources* 86 (2000) 442–448.
- [12] M.G. Pangalis, R.F. Martinez-Botas, N.P. Brandon, *Proc. Inst. Mech. Eng. Part A: J. Power Energy* 216 (2002) 129–144.
- [13] Y. Zhao, C. Ou, J. Chen, *Int. J. Hydrogen Energy* 33 (2008) 4161–4170.
- [14] S.H. Chan, K.A. Khor, Z.T. Xia, *J. Power Sources* 93 (2001) 130–140.
- [15] G.F. Naterer, C.D. Tokarz, J. Avsec, *Int. J. Heat Mass Transf.* 49 (2006) 2673–2683.
- [16] D.A. Noren, M.A. Hoffman, *J. Power Sources* 152 (2005) 175–181.
- [17] S.T. Ro, J.L. Sohn, *J. Power Sources* 167 (2007) 295–301.
- [18] Y. Qi, B. Huang, K.T. Chuang, *J. Power Sources* 150 (2005) 32–47.
- [19] F. Calise, A. Palombo, L. Vanoli, *J. Power Sources* 158 (2006) 225–244.
- [20] Y. Ji, K. Yuan, J.N. Chung, Y.C. Chen, *J. Power Sources* 161 (2006) 380–391.
- [21] H. Zhu, R.J. Kee, *J. Power Sources* 117 (2003) 61–74.
- [22] S.J. Watowich, R.S. Berry, *J. Phys. Chem.* 90 (1986) 4624–4631.
- [23] C. Wang, M.H. Nehrir, S.R. Shaw, *IEEE Trans. Energy Convers.* 20 (2005) 442–451.
- [24] A. Haddad, R. Bouyekhf, A.E. Moudni, M. Wack, *J. Power Sources* 163 (2006) 420–432.
- [25] M.V. Williams, H.R. Kunz, J.M. Fenton, *J. Electrochem. Soc.* 152 (2005) A635–A644.
- [26] B. Dalslet, P. Blennow, P.V. Hendriksen, N. Bonanos, D. Lybye, M. Mogensen, *J. Solid State Electrochem.* 10 (2006) 547–561.
- [27] Z. Zhang, X. Huang, J. Jiang, B. Wu, *J. Power Sources* 161 (2006) 1062–1068.
- [28] F. Calise, M. Dentice d'Accadia, A. Palombo, L. Vanoli, *Energy* 31 (2006) 3278–3299.
- [29] M. Sorrentino, C. Pianese, Y.G. Guezennec, *J. Power Sources* 180 (2008) 380–392.
- [30] J. Larminie, A. Dicks, *Fuel Cell Systems Explained*, 2nd ed., Wiley, New York, 2003.
- [31] S.H. Chan, Z.T. Xia, *J. Appl. Electrochem.* 32 (2002) 339–347.
- [32] I. Barin, O. Knacke, *Thermochemical Properties of Inorganic Substances*, Springer, Berlin, 1973, Suppl., 1997.
- [33] S. Wang, C. Xie, Y. Wang, L. Zhang, W. Jie, S.J. Hu, *J. Power Sources* 169 (2007) 338–346.
- [34] L.H. Zhang, Y. Liu, H.M. Song, S.X. Wang, Y.Y. Zhou, S.J. Hu, *J. Power Sources* 162 (2006) 1165–1171.
- [35] A.J. Appleby, F.R. Foulkes, *Fuel Cell Handbook*, Van Nostrand Reinhold, New York, 1989.
- [36] F.P. Holman, *Thermodynamics*, McGraw-Hill, New York, 1969.
- [37] A.E. Lutz, R.S. Larson, J.O. Keller, *Int. J. Hydrogen Energy* 27 (2002) 1103–1111.
- [38] J. Chen, *J. Appl. Phys.* 72 (1992) 3778–3780.
- [39] A. Durmayaz, O.S. Sogutb, B. Sahinc, H. Yavuz, *Prog. Energy Combust. Sci.* 30 (2004) 175–217.
- [40] P.G. Bavarsad, *Int. J. Hydrogen Energy* 32 (2007) 4591–4599.
- [41] S.H. Chan, O.L. Ding, *Int. J. Hydrogen Energy* 30 (2005) 167–179.
- [42] D. Sánchez, R. Chacartegui, A. Muñoz, T. Sánchez, *J. Power Sources* 160 (2006) 1074–1087.
- [43] D. Sánchez, A. Muñoz, T. Sánchez, *J. Power Sources* 169 (2007) 25–34.
- [44] S. Sieniutycz, *Prog. Energy Combust. Sci.* 29 (2003) 193–246.
- [45] D.A. Blank, G.W. Davis, C. Wu, *Energy* 19 (1994) 125–133.
- [46] S. Bhattacharyya, D.A. Blank, *Int. J. Energy Res.* 24 (2000) 539–547.
- [47] D.A. Blanka, *J. Appl. Phys.* 84 (1998) 2385–2392.
- [48] K.J. Yoon, P. Zink, S. Gopalan, U.B. Pal, *J. Power Sources* 172 (2007) 39–49.
- [49] X. Zhang, G. Li, J. Li, Z. Feng, *Energy Convers. Manage.* 48 (2007) 977–989.
- [50] S. Cordiner, M. Feola, V. Mulone, F. Romanelli, *Appl. Therm. Eng.* 27 (2007) 738–747.
- [51] P. Costamagna, A. Selimovic, M. Del Borghi, G. Agnew, *Chem. Eng. J.* 102 (2004) 61–69.
- [52] H. Zhu, R.J. Kee, V.M. Janardhanan, O. Deutschmann, D.G. Goodwin, *J. Electrochem. Soc.* 152 (2005) A2427–A2440.